IJIE

UTHM Penerbit
Universiti Tun Hussein Onn Malaysia

INTERNATIONAL JOURNAL OF INTEGRATED ENGINEERING
ISSN: 2229-838X e-ISSN: 2600-7916

Vol. 18 No. 2 (2026) 294-306
https://publisher.uthm.edu.my/ojs/index.php/ijie

# Aerodynamic Performance Evaluation of Contemporary Passenger Vehicle Designs Using CFD

**Li Chuhui[1,2], Hidayatullah Mohammad Ali[3,4*]**

[1] *School of Mechanical and Electrical Engineering, Hainan Vocational University of Science and Technology, No. 18 Qiongshan Avenue, Meilan District, Haikou City, Hainan Province, 571125, CHINA*

[2] *Faculty of Engineering, City University Malaysia, Cyberjaya Campus, 3500, Jalan Teknokrat 3, Cyber 4, Cyberjaya, Selangor Darul Ehsan, 63000, MALAYSIA*

[3] *Department of Aerospace Engineering, Faculty of Engineering, Universiti Putra Malaysia, UPM Serdang, Selangor Darul Ehsan, 43400, MALAYSIA*

[4] *Aerospace Malaysia Research Centre (AMRC), Level 7, Tower Block, Faculty of Engineering, Universiti Putra Malaysia, UPM Serdang, Selangor Darul Ehsan, 43400, MALAYSIA*

*Corresponding Author: hidayatullah@upm.edu.my
DOI: https://doi.org/10.30880/ijie.2026.18.02.023

**Article Info**

Received: 15 November 2025
Accepted: 1 April 2026
Available online: 16 June 2026

**Keywords**

Aerodynamic performance, drag coefficient, pressure distribution, CFD simulations, electric vehicles

**Abstract**

Modern automotive design faces the challenge of reducing aerodynamic drag while meeting strict environmental standards and maintaining practicality, aesthetics, and efficiency in electric vehicles. This study investigates the aerodynamic performance of various vehicle body designs using Computational Fluid Dynamics (CFD) simulations, aiming to assess how design modifications influence drag reduction and pressure distribution across critical surfaces. Simulations were conducted at various speeds to evaluate the aerodynamic behavior of each design, focusing on the drag coefficient and pressure values in key areas such as the front end, windshield, roof, and rear section. Results showed that one configuration achieved a significant improvement in aerodynamic efficiency, with the drag coefficient reduced to 0.273 at 30 km/h and further to 0.259 at 120 km/h, demonstrating stable performance at both low and high speeds. Pressure values in critical regions also dropped substantially, with front-end pressure decreasing by more than 60% compared to other models. These reductions in aerodynamic resistance correlate directly with improved energy efficiency, benefiting both fuel-powered and electric vehicles. Notable aerodynamic improvements stemmed from smoother body contours, optimized roof curvature, and proportioned dimensions that enhance airflow and reduce turbulence. These design elements minimize flow separation and wake formation, resulting in reduced drag forces and better vehicle stability. This research underscores the importance of incorporating aerodynamic principles early in vehicle design, offering valuable insights for the development of energy-efficient, environmentally responsible vehicles and a practical framework for future automotive advancements.

## 1. Introduction

Aerodynamic performance has become an essential factor in modern automobile design as it directly affects fuel efficiency, driving stability, and noise reduction [1-2]. With stricter environmental regulations and the increasing demand for energy-saving vehicles, reducing the drag coefficient ($C_d$) has become a major concern for both manufacturers and researchers [3]. Although the concept of aerodynamics in vehicle design dates back to the early 20th century, advancements such as computational fluid dynamics (CFD) technology have significantly enhanced the understanding of airflow behavior and its impact on vehicle performance [4-6].

Several scholars have extensively investigated the aerodynamic performance of vehicles, employing various computational and experimental methods to optimize design features. In 2010, Mitra [7] investigated the impact of aerodynamic devices on a hatchback car under various wind conditions using wind tunnel testing. The study shows that adding rear spoilers significantly reduces the lift coefficient with almost no change in drag. Front spoilers or air dams slightly reduce lift but cause a small increase in drag. These aerodynamic additions improve vehicle stability, which is why such features are used in racing cars to enhance road grip.

In 2012, Raju et al. [8] introduced a foldable rear drag reduction device designed to lower the drag coefficient at the vehicle's rear, demonstrating its effectiveness in minimizing aerodynamic resistance. The same year, Sriram et al. [9] proposed a high-downforce airfoil for racing car rear wings, aiming to enhance rear downforce while maintaining aerodynamic balance. In 2016, Parmar et al. [10] compared various passenger car deflectors through wind tunnel and CFD analysis, revealing that the design and positioning of spoilers significantly affect aerodynamic forces. In 2017, Azmi et al. [11] utilized 3D CFD analysis with ANSYS Fluent to study general-purpose utility vehicle design, successfully reducing turbulent energy by controlling airflow differences at the top and rear of the vehicle.

In 2018, Satishkumar et al. [12] investigated the effect of rear spoilers on hatchback models using wind tunnel testing. The proposed collapsible wind friction reduction attachment (C.W.F.R.A.) for the rear of a car helps reduce aerodynamic drag, improving fuel efficiency and allowing higher speeds without increasing engine capacity. Its collapsible design minimized problems related to parking space, city traffic, and driving on narrow or hilly roads compared to fixed devices. Additionally, modifying the overdrive gearbox can increase vehicle speed by about 1.3 times without raising engine speed, improving efficiency, and reducing emissions. In the same year, Wang et al. [13] analyzed racing car aerodynamics through CFD and wind tunnel methods, defining six critical aerodynamic components and validating the accuracy of their CFD simulations against experimental data.

In 2021, Nath et al. [14] evaluated the impact of aerodynamic devices on vehicle resistance through continuous development of vehicle aerodynamics, which has led to the devices improving in efficiency and reducing fuel consumption. The study used numerical simulation to analyze a baseline GT car with various add-on aerodynamic devices, showing that drag can be reduced by keeping airflow attached to the body. The GT spoiler with diffuser achieved the highest drag reduction of 16.53%, while other devices like fins improved stability and wings increased downforce but also added drag. Proper optimization of these devices can enhance vehicle aerodynamics in different driving conditions.

In 2022, Afianto et al. [15] applied CFD modeling to optimize the aerodynamic features of electrical hatchbacks. Their work showed that devices such as front spoilers, rear diffusers, and fins effectively reduced drag by 10% and lift by 73%, improving range, stability, and handling at high speeds. In the same year, Al-Saadi [16] used CFD to improve the aerodynamic performance of the Land Rover Discovery by testing four turbulence models, where the Realizable $k-\varepsilon$ model showed the most accurate results. The combined use of a ventilation duct and roof modification reduced the drag coefficient to 0.382791 and the lift coefficient to -0.153046, enhancing fuel efficiency and high-speed stability compared to the baseline model.

In 2023, Piratla [17] studied how aerodynamic modifications like spoilers, diffusers, and curved front bumpers affect passenger vehicles using CFD analysis. The findings showed an average 16% reduction in drag coefficient and a 232% reduction in lift coefficient, with the best drag improvement in hatchbacks and the highest lift improvement in sedans and SUVs. In 2024, Isah et al. [18] used CFD analysis to study how changing the front hood angle of a passenger vehicle affects its aerodynamics. The results showed that adjusting the hood angle reduced the drag coefficient by 7.72% and the lift coefficient by 33.3%. In the same year, Goel et al. [19] compared the aerodynamic performance of sedans, SUVs, and hatchbacks using CFD simulations and wind tunnel testing. The study analyzed pressure distribution and drag forces for each vehicle type, providing insights into how body geometry affects aerodynamic efficiency and helps improve fuel economy and overall vehicle performance. In 2025, Quispe and Velarde [20] applied CFD using ANSYS Fluent to analyze a sedan's external aerodynamics, accurately predicting flow behavior, pressure distribution, and wake formation with a drag coefficient of 0.312. The study identified rear-end and underbody regions as key contributors to drag, suggesting design improvements such as diffusers and spoilers for further reduction.

Although many studies have investigated aerodynamic optimization in conventional passenger cars, research that is tailored specifically to electric vehicles remains comparatively limited. This distinction is important because electric vehicles have different design priorities. Reducing aerodynamic drag not only influences performance but also directly extends driving range and improves energy efficiency. Recent studies have often focused on isolated components or have relied on geometries that were originally developed for conventional cars. What is still lacking is a comprehensive analysis that considers multiple design elements together, including the overall body shape, underbody flatness, spoilers, and air guides, within the context of electric vehicle requirements. The present study addresses this gap by performing CFD simulations on modern electric vehicle designs to develop practical aerodynamic optimization strategies that can improve efficiency, stability, and environmental performance. While some of the findings may also be relevant to conventional vehicles, the focus of this work is on providing solutions that are directly applicable to the unique design and operational demands of electric vehicles.

## 2. Methodology

This research adopted a structured and comprehensive methodology to design, simulate, and evaluate the aerodynamic performance of a newly developed vehicle model compared with a pre-existing commercially available model. The process involved the design of vehicle geometries, computational domain setup, mesh generation, turbulence modeling, solver configuration, and post-processing analysis to derive meaningful aerodynamic performance indicators.

### 2.1 Design Development

The development of the vehicle design began by focusing on embracing the front and rear parts of the car body. The design of the front end was carefully modeled to adopt a U-shaped structure, which was inspired by the Xpeng P7i (as depicted in Fig. 1(a)). This approach aimed to streamline the flow of air along the vehicle's surface, reduce the stagnation pressure at the nose, and encourage laminar flow behavior. The final U-shaped design for the new model, as seen in Fig. 1(b), successfully integrated these principles, ensuring a smooth transition from the front bumper to the windshield region.

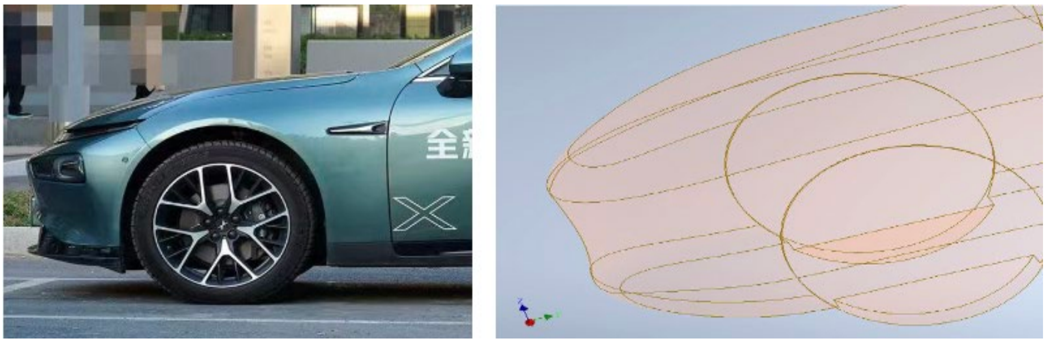

**(a)** **(b)**

**Fig. 1** *U-shaped front design of (a) Xpeng P7i; and (b) Proposed model*

Attention was also given to the rear-end design, where flow separation and wake formation traditionally contribute to high-pressure drag. The rear geometry of the new model was refined based on the design of the Porsche Panamera, as shown in Fig. 2(a), to promote gradual pressure recovery and reduce the wake region size. The actual rear design of the proposed model is illustrated in Fig. 2(b), which demonstrates the tapering and curvature adjustments introduced to control the airflow detachment behavior effectively.

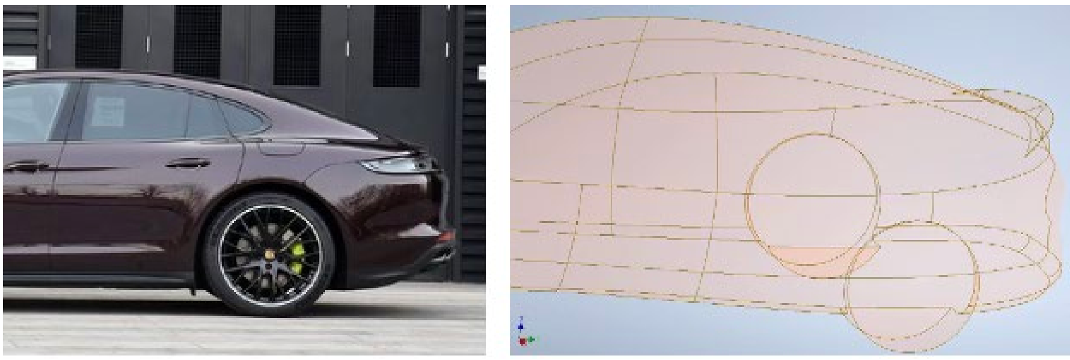

**(a)** **(b)**

**Fig. 2** *Rear design of (a) Porsche Panamera; and (b) Proposed model*

A comprehensive view of the entire newly designed car model is presented in Fig. 3. This diagram confirms the incorporation of both the front and rear aerodynamic enhancements, aimed at reducing the overall drag coefficient while maintaining practical design constraints typical of passenger vehicles. The selection of comparison models was carefully made to ensure a valid and reliable evaluation of the newly designed fastback sedan. Fastback sedans were specifically chosen because of their aerodynamic form and styling closely match the design philosophy of the new model, allowing for a meaningful assessment of aerodynamic performance differences.

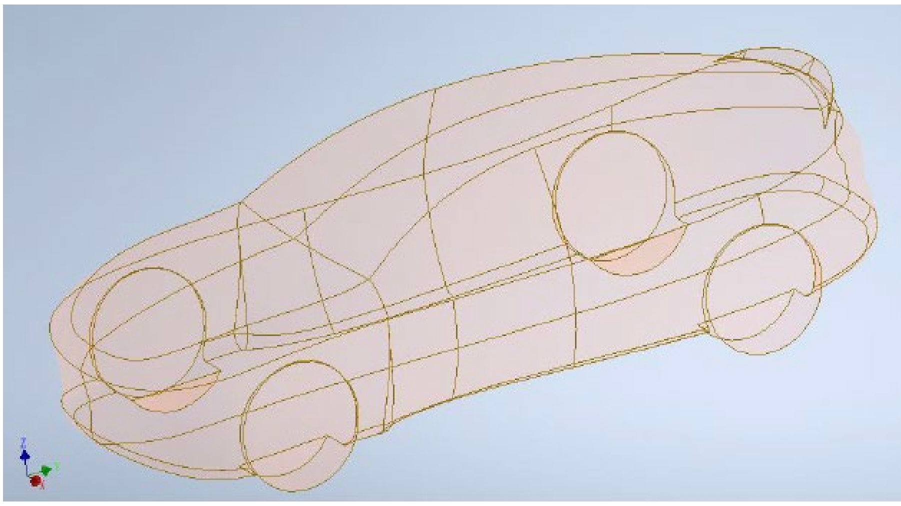

**Fig. 3** *Proposed car model No. 3 diagram*

To maintain computational efficiency and reduce simulation time, the comparison models were simplified by excluding intricate geometric details that do not significantly affect overall aerodynamics. Additionally, the body dimensions of the comparison models with 5 m in length, 2 m in width, and 1.5 m in height were matched exactly to the new design, as shown in Fig. 4. This size consistency eliminated variables related to scale effects, ensuring that differences in aerodynamic performance arose purely from design features such as body contours and roof slopes. This precise selection strategy provided a focused and accurate basis for evaluating and optimizing the aerodynamic qualities of the new vehicle model.

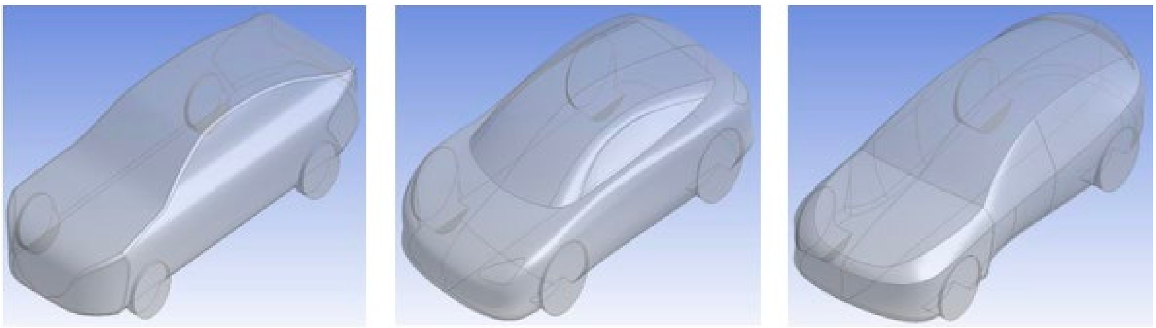

**(a)** **(b)** **(c)**

**Fig. 4** *Car geometry models of (a) Car No. 1; (b) Car No. 2; and (c) Car No. 3*

## 2.2 Computational Domain Setup

Subsequently to the completion of model geometry, the respective CAD files were imported into ANSYS Fluent for CFD analysis. Next, the computational domain was constructed to replicate realistic driving conditions, as shown in Fig. 5. This simulation was constructed as a regular three-dimensional rectangular space to capture the detailed flow characteristics around the vehicle, especially in its rear region, where complex aerodynamic phenomena such as vortices and backflow occur.

To ensure stable airflow development before reaching the vehicle, the inlet boundary was positioned 10 m in front of the car. The outlet boundary was set 20 m behind the vehicle, equivalent to four times the vehicle's length, to allow sufficient space for wake development and flow stabilization. The total width of the domain was set to 6 m, with the vehicle placed precisely at the center. Since the vehicle body width is approximately 2 m, centering the model provided about 2 m of clearance between each vehicle side and the domain side walls, which ensured adequate space for lateral airflow development. Boundary conditions included a velocity as air exited the domain, and wall boundaries on the remaining surfaces to mimic environmental obstructions, as shown in Table 1. The working fluid was defined as air, representing actual driving conditions. Here, the CFD simulations were conducted under standard atmospheric conditions, where the air density was assumed to be 1.225 $kg/m^3$ and the dynamic viscosity was $1.789 \times 10^{-5} Pa \cdot s$. These values correspond to air at approximately 25 $°C$ and 1 atm pressure and are commonly used as a default parameter in simulations where air is treated as an incompressible fluid.

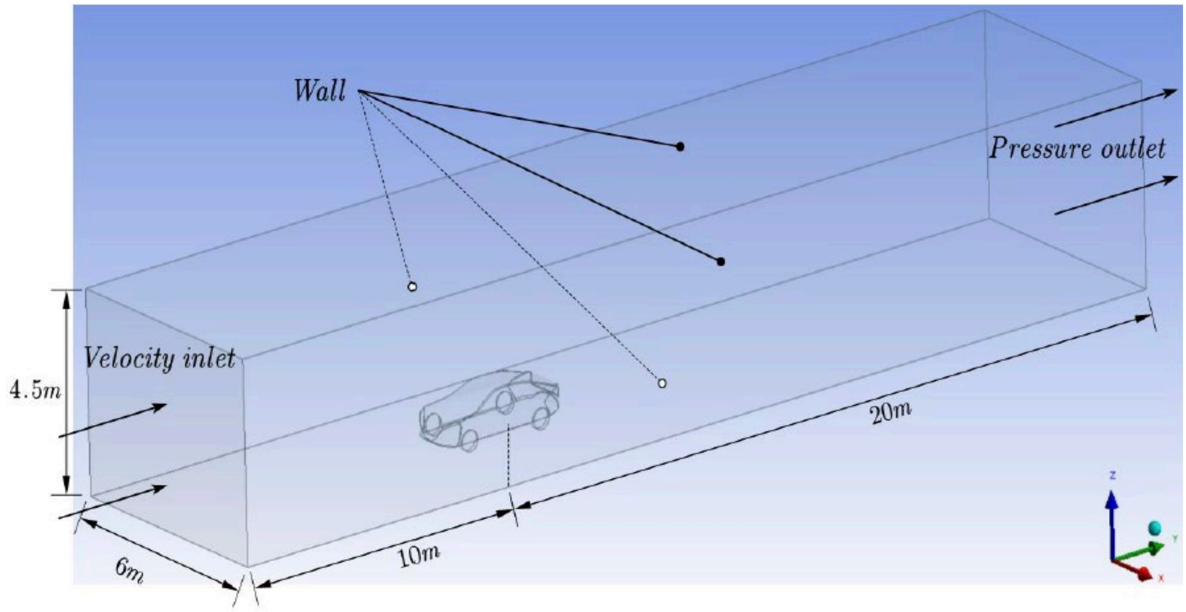


**Fig. 5** *Vehicle simulation domain using car No. 1 as an example*

**Table 1** *Boundary conditions*

| Boundary conditions | Type |
|---|---|
| Inlet | Velocity-inlet |
| Outlet | Pressure-outlet |
| Car | Wall |
| Wall(s) | Wall |
| Interior surface body | Interior |
| Surface body | Interior |

## 2.3 Mesh Strategy

After constructing the computational domain, the meshing process was performed using the Workbench-Mesh module, which efficiently generated high-quality unstructured grids dominated by quadrilaterals with some triangles. This mesh type was particularly suitable for capturing the complex and irregular geometry of the car body, including curves, joints, and aerodynamic features at the front and rear. The mesh ensured smooth transitions between cells, minimizing numerical errors and preserving the accuracy of the simulation results. Fig. 6 shows the generated mesh for Car No. 1, showing the detailed grid distribution.

A grid quality indicator was conducted using four mesh densities with cell sizes of 0.8 m, 0.6 m, 0.4 m, and 0.2 m. The analysis compared orthogonal quality, skewness, and aspect ratio across these grids. Based on Table 2, the results revealed minimal differences in grid quality indicators despite the increase in element count from 1.2 million to 1.7 million, indicating that further refinement had little effect on result accuracy but significantly increased computational time. To balance accuracy and efficiency, a cell size of 0.4 m was selected for the final simulations, as it provided sufficient grid quality without high computational cost.

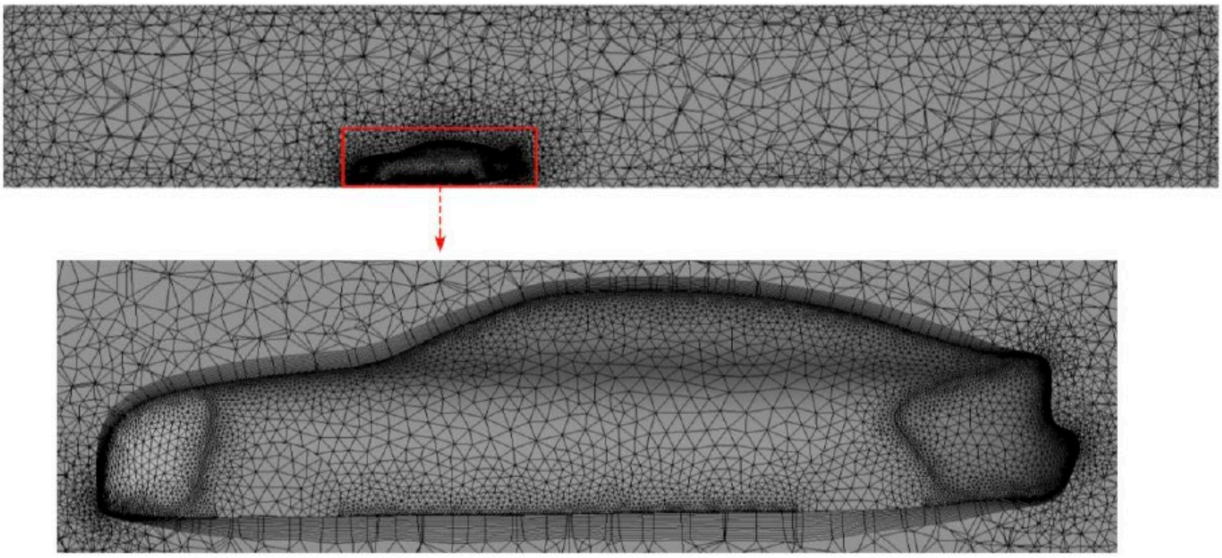

**Fig. 6** *Schematic diagram of grid division using car No. 1 as an example*

**Table 2** *Grid quality indicators*

| Mesh No. | Element Size (m) | Elements | Orthogonal Quality | Skewness | Aspect Ratio |
|---|---|---|---|---|---|
| 1 | 0.8 | 1,203,719 | 0.769 | 0.229 | 8.816 |
| 2 | 0.6 | 1,224,874 | 0.769 | 0.229 | 8.612 |
| 3 | 0.4 | 1,290,420 | 0.769 | 0.229 | 8.293 |
| 4 | 0.2 | 1,741,995 | 0.770 | 0.228 | 6.640 |

## 2.4 Turbulence Modeling and Solver Configuration

In this study, turbulence modeling and numerical solution configuration were conducted with careful consideration to ensure the accuracy and reliability of the simulation results, as shown in Table 3. The Shear Stress Transport k-omega (SST k-$\omega$) turbulence model was selected for all vehicle simulations. This model was chosen because it integrates the advantages of both the standard k-omega and the standard k-epsilon model, providing superior performance in capturing the complex turbulent structures present around automobile geometries.

**Table 3** *Solver setting*

| General | |
|---|---|
| Type | Pressure-based |
| Velocity formulation | Absolute |
| Time | Steady-state |
| 3D space | Planar |
| **Model** | |
| Viscous | SST k-omega |
| **Reference values** | |
| Density (kg/m3) | 1.225 |
| Pressure (pascal) | 101325 |
| Temperature (K) | 288.16 |
| Velocity (km/h) | 30, 60, 90, 120 |
| Viscosity (kg/m-s) | 1.789e-005 |
| **Solution** | |
| Method | Pressure-velocity coupling |
| Scheme | Coupled |
| Residual error | 1.e-006 |

It is particularly effective in resolving near-wall flows, flow separation, and wake formation, which are critical to accurately predicting aerodynamic drag and lift forces. For solving the governing fluid flow equations, the Semi-Implicit Method for Pressure-Linked Equation (SIMPLE) algorithm was utilized. The SIMPLE algorithm is a widely validated numerical method known for its robust convergence characteristics and its ability to handle pressure-velocity coupling in steady-state simulations. Each simulation was set up to undergo a maximum of 800 iterations to ensure that the solution reached a fully converged state. Convergence was assessed not only by monitoring residuals but also by checking the stabilization of aerodynamic coefficients. Once these parameters no longer changed with additional iterations, the solution was considered converged. Test runs extended beyond 800 iterations showed no noticeable variation in the results, further confirming that this iteration limit was sufficient. These solver settings, combined with the turbulence model, provided a dependable framework for capturing the aerodynamic behavior of the vehicle under various driving speeds of 30 km/h, 60 km/h, 90 km/h, and 120 km/h.

## 2.5 Result Interpretation and Aerodynamic Performance Evaluation

Post-processing of simulation data was performed with a focus on extracting and analyzing aerodynamic performance indicators critical to vehicle design evaluation. Key aerodynamic parameters such as the drag coefficient ($C_d$), pressure distribution, and flow velocity fields were derived from the simulation outputs. To accurately capture localized flow characteristics and compare performance among the different vehicle models, a series of pressure monitoring points was strategically placed along the central longitudinal section of each vehicle. This arrangement ensured that the collected data was consistent, representative, and directly comparable between models. Additionally, the overall aerodynamic efficiency was assessed by evaluating the drag coefficient values under each of the tested speed conditions. The post-processing phase thus provided a comprehensive understanding of the aerodynamic strengths and weaknesses of the newly designed vehicle relative to the benchmark models. The schematic layout of these monitoring points, shown in Fig. 7, served as a vital reference for interpreting the spatial distribution of aerodynamic forces and for supporting the later detailed analysis. Although Fig. 7 represents the monitoring point arrangement for car No. 1, the same layout was consistently applied to car No. 2 and car No. 3 in order to ensure comparability across all models.

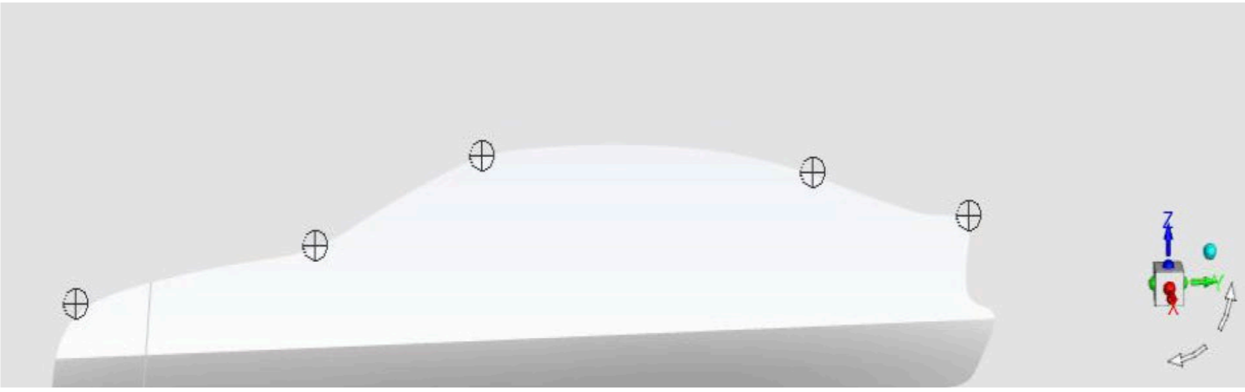

**Fig. 7** *Schematic diagram of monitoring point locations for car No. 1*

## 3. Results and Discussion

This section presents a computational analysis of the aerodynamic performance of three vehicle models. Car No. 1 and car No. 2 serve as reference designs, while car No. 3 represents the newly optimized configuration developed in this study. Using CFD simulations, the study evaluates pressure distributions over critical vehicle surfaces and assesses the resulting drag coefficient. The design of car No. 3 incorporates targeted modifications, including a U-shaped front section, optimized windshield and roof curvature, and an enlarged rear diffuser, all aimed at reducing aerodynamic resistance.

## 3.1 Front Pressure

The front surface of a vehicle is the primary point of contact with incoming airflow and typically experiences the highest stagnation pressure, directly influencing pressure drag. The term front pressure refers to the pressure acting on the entire frontal surface of the vehicle, which includes the grille region, bumper, and surrounding components. This surface represents the initial contact zone with oncoming airflow and therefore plays a significant role in determining overall aerodynamic drag. According to CFD simulation results, as shown in Fig. 8, car No. 3 demonstrates a significant reduction in front surface pressure compared to the two reference models across all tested speeds. At a lower speed of 30 km/h, the front pressure measured on car No. 3 is 3.175 Pa, while car No. 1 registers 9.799 Pa and car No. 2 records 11.450 Pa. This reduction corresponds to approximately 67.6% compared to car No. 1 and about 72.3% compared to car No. 2, highlighting the substantial benefit achieved even at moderate speeds.

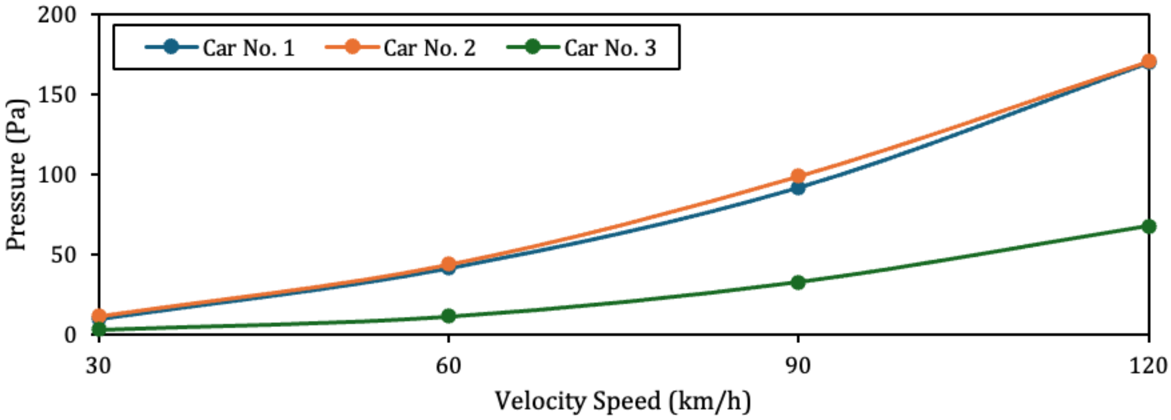


**Fig. 8** *Front pressure versus velocity for different car designs*

As speed increases to 120 km/h, the front pressure naturally rises due to the quadratic relationship between speed and dynamic pressure. Nonetheless, car No. 3 continues to maintain a lower front pressure of 67.424 Pa, in contrast to 169.276 Pa for car No. 1 and 170.33 Pa for car No. 2. The difference at this higher speed equates to around 60% lower front pressure relative to both reference models. This consistent advantage stems from the U-shaped front-end design of car No. 3, which ensures smoother airflow transition around the nose section and delays the onset of flow separation, thereby reducing stagnation zones that contribute heavily to frontal aerodynamic resistance.

Beyond numerical reduction itself, the implications are significant, with a lower front pressure meaning less force resisting forward motion, leading to a directly measurable decrease in pressure drag. This design choice not only benefits energy consumption at cruising speeds but also supports better airflow distribution toward downstream sections of the vehicle body, which can further reduce drag and improve stability.

## 3.2 Front Windshield Pressure

The front windshield serves as a critical aerodynamic transition zone, channeling airflow from the vehicle hood onto the roof. CFD simulations presented in Fig. 9 show that the newly designed car No. 3 achieves consistently lower front windshield surface pressures compared to car No. 1 across all tested speeds. At the highest test speed of 120 km/h, the front windshield pressure recorded for car No. 1 was 237.590 Pa, whereas car No. 3 achieved a substantially reduced pressure of 140.125 Pa. This represents a reduction of 97.465 Pa, corresponding to an improvement of approximately 41.0 percent relative to a baseline. At 90 km/h, the pressure on car No. 1 was 134.002 Pa, while car No. 3 recorded 78.962 Pa, yielding an equally significant reduction of 41.0%. Similar trends appear at lower speeds, with car No. 3 consistently showing about 40% lower pressure compared to car No. 1.

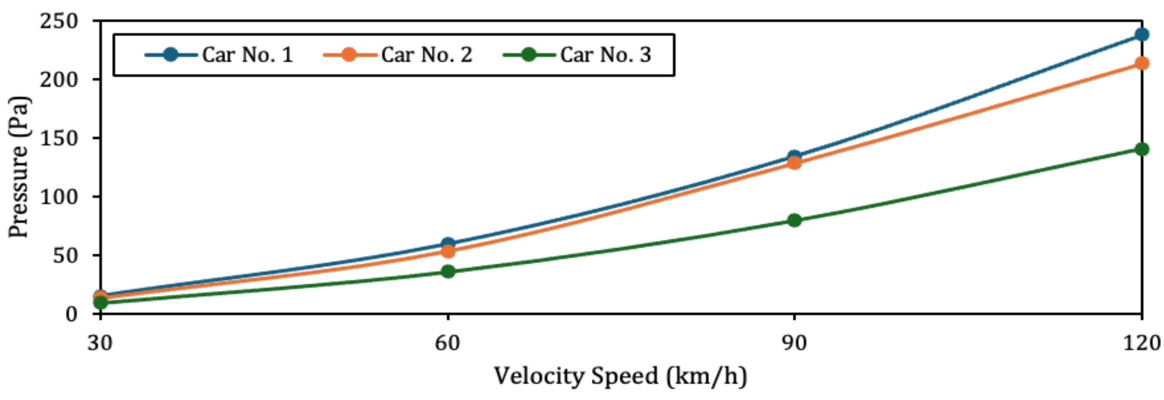


**Fig. 9** *Front windshield pressure versus velocity for different car designs*

Int. Journal of Integrated Engineering Vol. 18 No. 3 (2026) p. 294-306

The aerodynamic improvement is attributed to the more refined curvature and inclination of the front windshield in car No. 3, which helps maintain airflow attachment and delays separation. Lower windshield pressure reduces aerodynamic lift on the front axle, which contributes to better vehicle stability, especially at higher speeds. Additionally, smoother airflow over the windshield minimizes turbulence that can cause wind noise, enhancing driver and passenger comfort. Importantly, these gains were achieved without altering the overall styling language or compromising regulatory requirements for visibility. This demonstrates the practical value of using CFD-guided design to optimize a single surface for measurable aerodynamic benefit.

## 3.3 Roof Pressure

The roof section continues the aerodynamic pathway established by the windshield and plays an equally important role in sustaining attached flow towards the rear of the vehicle. According to the CFD results provided in Fig. 10, car No. 3 demonstrates significantly reduced roof surface pressure across all tested speeds. At 120 km/h, car No. 1 recorded a roof pressure of 521.644 Pa, whereas car No. 3 measured 337.209 Pa, representing a reduction of 184.435 Pa or approximately 35.4% lower pressure relative to the baseline. At 90 km/h, car No. 1 recorded 287.748 Pa and car No. 3 had 189.197 Pa, a decrease of 98.551 Pa, which corresponds to 34.2% lower. Similar reductions of about 34% to 35% were observed at lower speeds.

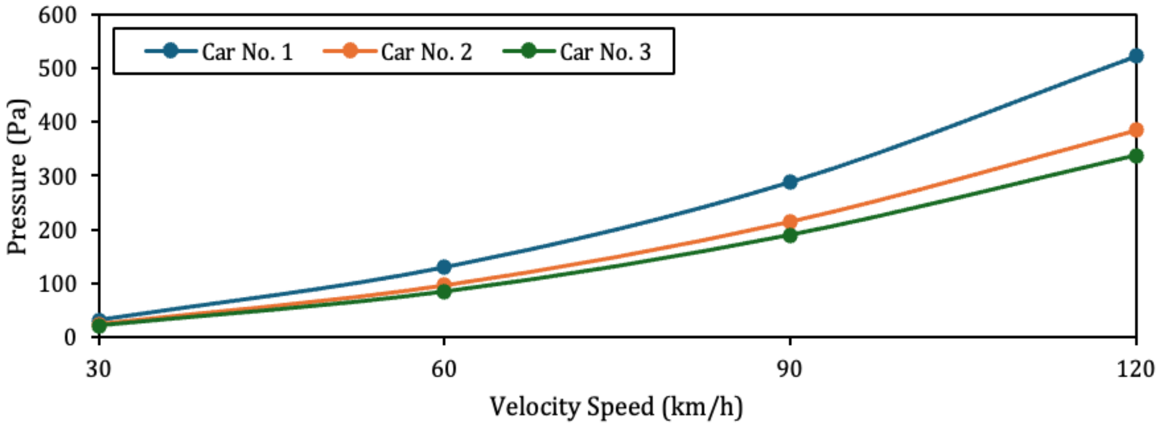


**Fig. 10** *Roof pressure versus velocity for different car designs*

This improvement results from the smoother and more continuous curvature of the roof in car No. 3, which reduces the adverse pressure gradient and maintains laminar flow over a larger area. Sustaining attached flow on the roof limits the formation of turbulent eddies, which not only lowers pressure drag but also reduces aerodynamic lift. This explains that the lower lift over the roof section contributes to greater high-speed stability and improved crosswind performance, which is important for passenger safety. Furthermore, these aerodynamic gains were achieved without sacrificing interior headroom, illustrating that careful design adjustments can produce meaningful performance benefits within practical packaging constraints.

## 3.4 Rear Windshield Pressure

The rear windshield is typically a challenging area for aerodynamic design because its downward slope can cause early flow separation and create low-pressure zones that increase drag. CFD simulations in Fig. 11 show that car No. 3 significantly lowers rear windshield pressure across all speeds tested. At 120 km/h, car No. 1 recorded a rear windshield pressure of 406.683 Pa, whereas car No. 3 achieved 127.246 Pa, representing a large reduction of 279.437 Pa or approximately 68.7% lower pressure compared to the baseline. At 90 km/h, the reduction reached 75.6%, with car No. 1 at 226.724 Pa and car No. 3 at 55.443 Pa. Similar substantial reductions of over 70% were observed even at lower speeds.

The attribution of this performance to the refined inclination angle of the rear windshield in car No. 3, which smooths the transition from the roof to the rear deck. This smoother geometry delays flow separation, narrows the wake region immediately behind the cabin, and raises base pressure. Higher rear windshield pressure reduces pressure drag and also helps control lift forces acting on the rear axle, which enhances overall stability during high-speed driving. The results demonstrate that rear windshield design, although occupying a relatively small area of the vehicle, has a disproportionately large impact on aerodynamic drag and stability.

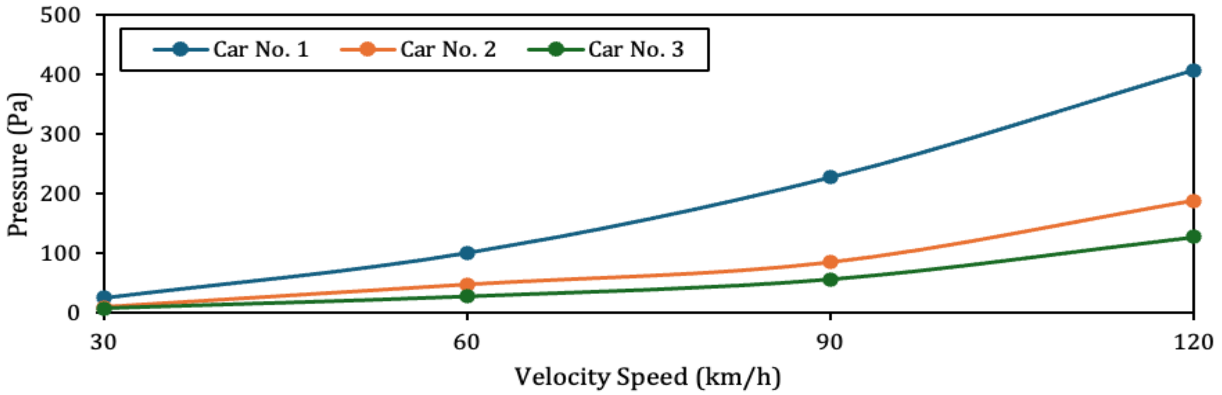


**Fig. 11** *Rear windshield pressure versus velocity for different car designs*

## 3.5 Rear Pressure

The rear surface of the vehicle is often the most influential region for total aerodynamic drag, as it directly determines the wake size and the resulting base pressure. The CFD data in Fig. 12 show that car No. 3 achieves markedly lower rear surface pressure compared to car No. 1. At 120 km/h, car No. 1 recorded a rear surface pressure of 224.443 Pa, whereas car No. 3 measured 48.443 Pa. This reduction of 176.000 Pa corresponds to an impressive 78.4% lower pressure relative to the baseline. At 90 km/h, car No. 1 had 118.848 Pa and car No. 3 had 35.848 Pa, yielding a reduction of 69.8%. Reductions above 58% were observed at lower speeds as well.

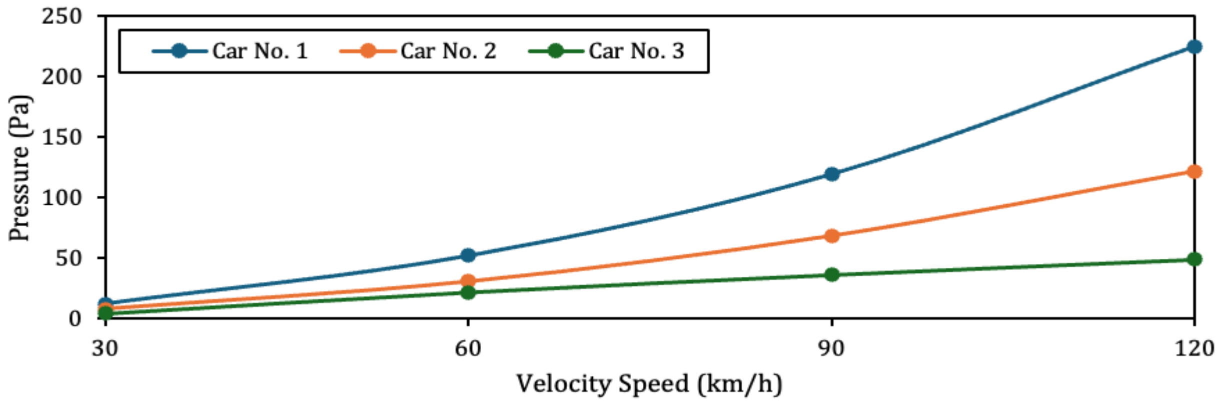


**Fig. 12** *Rear pressure versus velocity for different car designs*

This significant improvement is primarily due to the larger rear diffuser and smoother rear body geometry in car No. 3, which enhances flow detachment by channeling underbody and upper flow more effectively. By raising the rear base pressure, the pressure differential between the front and rear surfaces is reduced, which directly lowers pressure drag, the dominant component in sedan-type vehicles. This underlines that this aerodynamic refinement was accomplished without compromising trunk space or rear packaging, confirming the practical feasibility of integrating diffuser designs in modern vehicle platforms.

## 3.6 Drag Coefficient

The cumulative effect of these local pressure reductions is reflected in the overall drag coefficient. According to the CFD data in Fig. 13, car No. 1 exhibited an average drag coefficient of 0.269 at higher speeds, whereas car No. 3 achieved 0.204. This difference of 0.065 represents a reduction of approximately 24.2%. This magnitude of $C_d$ reduction is highly significant for real-world vehicle performance. A lower drag coefficient reduces the aerodynamic force that opposes vehicle motion, which improves fuel efficiency for internal combustion vehicles and extends the driving range of electric vehicles.

This improvement results not from a single design change but from coordinated reductions in surface pressures across the front, windshield, roof, rear windshield, and rear sections. The data highlight the effectiveness of using CFD as a design tool to systematically target and optimize each aerodynamic zone of the vehicle, leading to a measurable reduction in total drag.

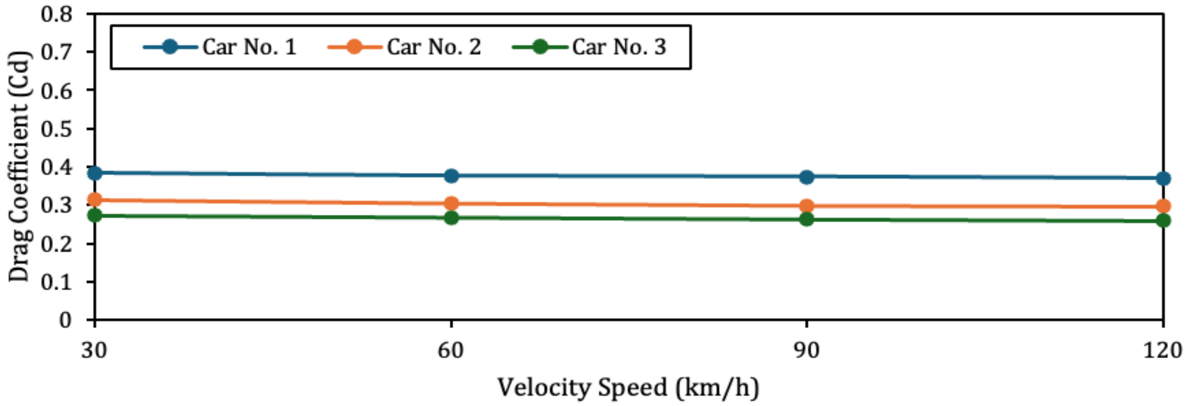


**Fig. 13** *Drag coefficient versus velocity for different car designs*

### 3.7 Integrated Discussion

When integrated, the CFD results demonstrate that car No. 3 achieves pressure reductions of approximately 60% at the front surface compared to car No. 1, reductions of about 34% to 41% at the front windshield and roof, and substantial reductions of around 68% to 78% at the rear windshield and rear surfaces. Together, these localized improvements contribute to a drag coefficient decrease of approximately 0.065, which corresponds to an overall improvement of about 24.2% relative to the baseline vehicle. This aerodynamic enhancement confirms that effective drag reduction relies on coordinated optimization of multiple vehicle surfaces rather than isolated design changes. The study further shows that carefully adjusting the front profile, windshield inclination, roof curvature, rear windshield slope, and rear diffuser geometry can produce quantifiable aerodynamic benefits. These results validate the effectiveness of using CFD to guide design decisions, demonstrating that targeted surface pressure reductions translate into measurable reductions in total drag. The findings also highlight how aerodynamic refinement can be achieved while retaining styling constraints and functional packaging, thereby supporting modern automotive goals of improved efficiency, reduced energy consumption, and enhanced high-speed stability.

## 4. Conclusion

This study used CFD simulations to evaluate the aerodynamic performance of three vehicle models and found that the newly designed car No. 3 achieved consistently lower drag coefficients, decreasing from 0.273 at 30 km/h to 0.259 at 120 km/h, compared to higher values recorded for car No. 1 and car No. 2. Detailed pressure analysis showed reductions of around 60% at the front surface, approximately 34% to 41% at the front windshield and roof, and up to 68% to 78% at the rear windshield and rear surfaces. These improvements result from coordinated design refinements that guide airflow more smoothly and reduce flow separation. By lowering both drag and aerodynamic lift, the study confirms that systematic exterior optimization supported by CFD can enhance vehicle efficiency and stability without compromising design or functionality. Importantly, because reducing drag directly contributes to extending range in electric vehicles, the results demonstrate that aerodynamic refinement is a practical strategy for improving the energy efficiency and environmental performance of EVs. While some of the principles may also apply to conventional cars, the emphasis of this work is on addressing the unique requirements of electric vehicle design. The results provide practical evidence that aerodynamic design remains a vital strategy for reducing wind resistance and supporting energy-saving goals in modern automotive engineering. While the present study focused on comparative CFD evaluation, future work should include validation against experimental data (e.g., wind tunnel testing or benchmark models such as DrivAer) and a convergence study based on aerodynamic parameters to complement the grid quality analysis and further validate the accuracy of the findings. Additionally, extending the analysis to a broader range of electric vehicle geometries and driving conditions could provide more comprehensive insights.

## Acknowledgement

The authors would like to thank the Department of Aerospace Engineering and *Aerospace Malaysia Research Centre (AMRC)*, Faculty of Engineering, University Putra Malaysia, for their academic and technical guidance throughout this research. The authors are also grateful to the School of Mechanical and Electrical Engineering, Hainan Vocational University of Science and Technology, for providing administrative support and computational resources. In addition, the authors acknowledge the Faculty of Engineering, City University Malaysia, for their academic guidance during the study.

## Conflict of Interest

The authors declare that there is no conflict of interest regarding the publication of the paper.

## Author Contribution

*The authors confirm contribution to the paper as follows:* ***study conception and design:*** *Li Chuhui, Hidayatullah Mohammad Ali;* ***data collection:*** *Li Chuhui;* ***analysis and interpretation of results:*** *Li Chuhui, Hidayatullah Mohammad Ali;* ***draft manuscript preparation:*** *Hidayatullah Mohammad Ali. All authors reviewed the results and approved the final version of the manuscript.*

## References

[1] Yang, X., Cai, Z., & Ye, Q. (2019). Aerodynamics analysis of several typical cars. *Journal of Engineering Thermophysics*, 28(2), 269-275. https://doi.org/10.1134/S1810232819020085

[2] Altinisik, A., Kutukceken, E., & Umur, H. (2015). Experimental and numerical aerodynamic analysis of a passenger car: Influence of the blockage ratio on drag coefficient. *Journal of Fluids Engineering*, *137*(8), 081104. https://doi.org/10.1115/1.4030183

[3] Muzir, N. A. Q., Mojumder, M. R. H., Hasanuzzaman, M., & Selvaraj, J. (2022). Challenges of electric vehicles and their prospects in Malaysia: A comprehensive review. *Sustainability*, *14*(14), 8320. https://doi.org/10.3390/su14148320

[4] Qin, P., Ricci, A., & Blocken, B. (2024). CFD simulation of aerodynamic forces on the DrivAer car model: Impact of computational parameters. *Journal of Wind Engineering and Industrial Aerodynamics*, *248*, 105711. https://doi.org/10.1016/j.jweia.2024.105711

[5] Nebot, E. P., Gupta, A., & Mahak, M. (2025). Investigating the Impact of Structural Features on F1 Car Diffuser Performance Using Computational Fluid Dynamics (CFD). *Mathematics*, *13*(9), 1455. https://doi.org/10.3390/math13091455

[6] Liu, Y. (2023). Harnessing CFD Modeling Techniques for Optimizing Automotive Streamlines and Reducing Aerodynamic Drag. *Highlights in Science Engineering and Technology*, 76, 212-221.

[7] Mitra, D. (2010). Effect of relative wind on notch back car with add-on parts. *International Journal of Engineering Science and Technology*, *2*(4), 472-476.

[8] Raju, D. K. M., Tech, M., & Reddy, G. J. (2012). A conceptual design of wind friction reduction attachments to the rear portion of a car for better fuel economy at high speeds. *International Journal of Engineering Science and Technology*, *4*(5), 2366-2372.

[9] Sriram, P. S., Gopalarathnam, A., & Misenheimer, A. (2012). High-downforce airfoil design for motorsports. *SAE International Journal of Materials and Manufacturing*, *5*(2), 478-489. https://doi.org/10.4271/2012-01-1168

[10] Parmar, M., Panchal, D., & Panchal, T. (2016). A Technical Review–Comparative Assessment of Aerodynamic Forces Generated Due to Wind Deflector of Passenger Car by CFD and Experimental Method. *International Journal of Engineering Research & Technology (IJERT)*, *4*(10).

[11] Azmi, M. F. M., Marzuki, M. A. B., & Bakar, M. A. A. (2017). Vehicle aerodynamics analysis of a multi-purpose vehicle using CFD. *ARPN Journal of Engineering and Applied Sciences*, *12*(7), 2345-2350.

[12] Sathishkumar, M., Nema, A., & Patel, K. D. (2018). Experimental analysis of aerodynamic drag reduction of a hatchback model car by rear spoiler in the wind tunnel. *International Journal of Mechanical and Production Engineering Research and Development (IJMPERD) 8.3 (2018): 991*, *1000*. https://doi.org/10.24247/ijmperdjun2018105

[13] Wang, J., Li, H., Liu, Y., Liu, T., & Gao, H. (2018). Aerodynamic research of a racing car based on wind tunnel test and computational fluid dynamics. In *MATEC Web of Conferences* (Vol. 153, p. 04011). EDP Sciences. https://doi.org/10.1051/matecconf/201815304011

[14] Nath, D. S., Pujari, P. C., Jain, A., & Rastogi, V. (2021). Drag reduction by application of aerodynamic devices in a race car. *Advances in Aerodynamics*, *3*, 1-20. https://doi.org/10.1186/s42774-020-00054-7

[15] Afianto, D., Han, Y., Yan, P., Yang, Y., Elbarghthi, A. F., & Wen, C. (2022). Optimisation and efficiency improvement of electric vehicles using computational fluid dynamics modelling. *Entropy*, *24*(11), 1584. https://doi.org/10.3390/e24111584

[16] Al-Saadi, A., Al-Farhany, K., Faisal, A. E., Alomari, M. A., Jamshed, W., Eid, M. R., ... & Amjad, A. (2022). Improvement of the aerodynamic behaviour of the passenger car by using a combine of ditch and base bleed. *Scientific reports*, *12*(1), 18462. https://doi.org/10.1038/s41598-022-23183-z

[17] Piratla, S. (2023). Evaluating the aerodynamics of different passenger vehicle configurations. *Authorea Preprints*. https://doi.org/10.36227/techrxiv.24139254.v1

[18] Isah, A., Abdulazeez, M. U., Aliyu, M., & Yahuza, I. (2024). Investigation of the Effect of a Passenger Vehicle Front Profile on Aerodynamic Performance. *Journal of Sustainable Engineering and Technology*, *1*(2), 215-224.

[19] Goel, V. K., Chopra, A., Tripathy, P., & Kumar, M. (2024). Aerodynamics studies of various passenger vehicles using computational fluid dynamics (CFD). *International Journal of Mechanical Engineering and Technology*, 15(6), 1-9.

[20] Quispe, C. P., & Velarde, J. E. (2025). CFD analysis of external aerodynamics of sedan car model using ANSYS Fluent. *International Journal of Automobile Engineering*, 6(1), 30-36.